ACS OMEGA

Open Access

http://pubs.acs.org/journal/acsodf

Article

Two-Step Hydrothermal Synthesis of Submicrometric and Hierarchical Hollow SAPO-34 with Superior Catalytic Performance in Methanol to Olefin (MTO) Reaction

Zhihui Guo, Kunlong Liu, Hui Wei, and Weiping Zhu*

Cite This: *ACS Omega* 2024, 9, 30321−30326

Read Online

ACCESS | Metrics & More | Article Recommendations | Supporting Information

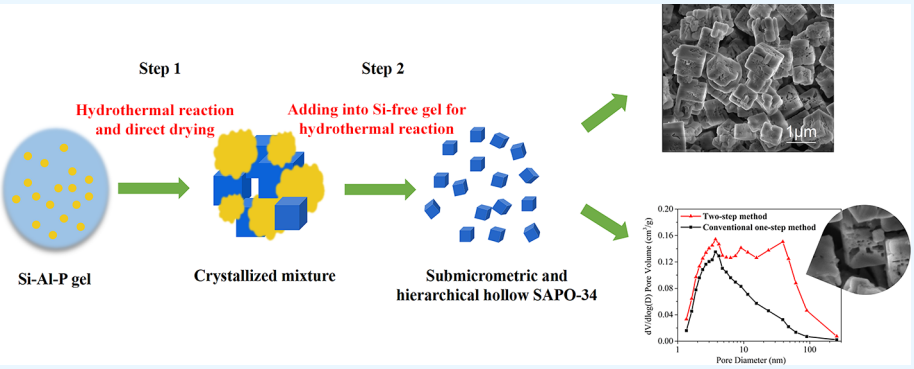

ABSTRACT: A submicrometric and hierarchical hollow SAPO-34 molecular sieve was synthesized by an easy and low-cost two-step hydrothermal method. First, the crystallized mixture was obtained by direct drying after a first-step hydrothermal reaction. Then, the SAPO-34 product was obtained by adding the crystallized mixture to silicon-free gel and using cheap and common template agents. Compared to conventional SAPO-34, the submicrometric and hierarchical hollow SAPO-34 exhibits superior catalytic activity in the MTO reaction.

1. INTRODUCTION

Silicoaluminophosphate molecular sieve SAPO-34, as a class of inorganic porous materials, shows excellent catalytic performance in MTO reaction as it possesses medium acidity, a unique CHA topological structure with eight ring pore openings (3.8 Å × 3.8 Å) and a large cavity (9.4 Å in diameter), and high hydrothermal stability.[1] However, SAPO-34 molecular sieves suffering from limitations of mass transport and rapid coke formation can result in partial coverage of the active sites in a short time. Therefore, the catalytic lifetime of SAPO-34 molecular sieves will be shortened.[2] To overcome the diffusion limitation and prolong the catalytic lifetime of molecular sieves in MTO reaction, researchers found that decreasing the crystal size, introducing a hierarchical structure, or a combination of both methods can shorten the diffusion path length and retard the formation of coke, thereby reducing the influence of diffusion limitation, prolonging the catalyst lifetime of SAPO-34 molecular sieves.[3]

Previous researchers have found a variety of methods to reduce crystal sizes, such as microwave-assisted synthesis,[4] ultrasonic-assisted synthesis,[5] crystal growth inhibitor-assisted synthesis,[6] dry gel conversion synthesis,[7] and adjustment of template agents.[8] The preparation of hierarchical SAPO-34 molecular sieves usually uses postsynthesis treatments such as dealumination or desilication methods[9] or uses soft-templates or hard templates.[10] However, the catalytic performance improvement by a single way to reducing the diffusion is not satisfied. Recently, small-sized and hierarchical SAPO-34 were studied extensively due to them possessing better catalytic performance. Some researchers have prepared hierarchical SAPO-34 nanocrystals.[11] However, the prices of the raw materials like organic template or cotemplate they used are higher than that of the traditional recipe. Besides, compared to nanosized hierarchical SAPO-34, submicrometric and hierarchical SAPO-34 is easy to be separated, thus reducing the cost of industrial production.[11b,12] Although the hydrothermal method is a common method for preparing SAPO-34, it is difficult to prepare submicrometric and hierarchical SAPO-34 only by the hydrothermal method and using the cheap and common template agent. Therefore, it is desirable to develop an easy and low-cost hydrothermal method to prepare

Received: February 8, 2024
Revised: June 11, 2024
Accepted: June 12, 2024
Published: July 2, 2024

submicrometer and hierarchical hollow SAPO-34 molecular sieves.

In this work, submicrometric and hierarchical hollow SAPO-34 have been prepared by a two-step hydrothermal method. The crystallized mixture obtained by direct drying after the first-step hydrothermal process can be used as the Si source and part of the Al and P sources in the hydrothermal process of the second step. The submicrometric and hierarchical hollow SAPO-34 exhibits long catalytic lifetime and superior selectivity for light olefin compared to conventional SAPO-34 molecular sieves in the MTO reaction.

2. EXPERIMENTAL SECTION

2.1. Synthesis of SAPO-34 Molecular Sieves. The precursor was synthesized with the molar composition of Al_2O_3:P_2O_5:SiO_2:TEA:DEA:H_2O = 1:1:*X*:2.6:0.72:45 (*X* = 0.6,1.2,1.8) under hydrothermal conditions at 200 °C for 24 h. The crystallized mixture was prepared by drying the precursor overnight at 120 °C, which was named Z1-0.6, Z1-1.2, and Z1-1.8 according to the ratio of SiO_2/Al_2O_3. Submicrometric and hierarchical hollow SAPO-34 was synthesized by adding the abovementioned crystallized mixture of different compositions into the synthesis of Si-free gels with the molar compositions of Al_2O_3:P_2O_5:TEA:DEA:H_2O = 1:1:2.6:0.72:45 under hydrothermal conditions at 200 °C for 24h. The solid products were collected by centrifugation, washed with deionized water, dried at 120 °C, and then calcined at 650 °C for 5 h. The obtained samples were named Z2-0.2, Z2-0.4, and Z2-0.6 according to the ratio of SiO_2 in the total solution. For comparison, the Z3-0.2 sample was synthesized with the molar composition of Al_2O_3:P_2O_5:SiO_2:TEA:DEA:H_2O = 1:1:0.2:2.72:0.75:45 by using the traditional optimized one-step hydrothermal method under the hydrothermal conditions at 200 °C for 24 h. Then, the solid product was collected by centrifugation, washed with deionized water, dried at 120 °C, and then calcined at 650 °C for 5h.

The yield of the products was calculated by the following equation:

$$\text{yield}(\%) = M_{\text{sample}} \times 85\% \times 100/(M_{\text{Al2O3+P2O5+SiO2}})\text{gel}$$

where M_{sample}, 85%, and $(M_{\text{Al2O3+P2O5+SiO2}})$ gel represent the product weight, the value estimation of the framework components in the sample, and the dried quantity of the inorganic oxides in the gel at the very beginning.

2.2. Characterization. The crystalline structure of the products before calcination was analyzed by powder X-ray diffraction (XRD) on a Bruker D8A (Bruker AXS GmbH, Karlsruhe, Germany) with monochromatic Cu Kα1 radiation (λ = 1.5406). The crystallinity is calculated by DIFFRAC.EVA software that divides baseline-corrected area into global area in the XRD patterns.

SEM photographs were obtained on an FEI Nova NanoSEM 450 scanning electron microscope (FEI Co., Hillsboro, Oregon, USA).

The chemical composition of the sample was determined by X-ray fluorescence (XRF) on an XRF-ZSX Primus II spectrometer (Rigaku Co., The Woodlands, Texas, USA).

The acidity of the samples was also studied by NH_3 temperature-programmed desorption (NH_3-TPD) on an AutoChem II 2920 TPD analyzer. 0.2 g of sample was first pretreated at 550 °C for 30 min in He flow to remove adsorbed water. Subsequently, the sample was cooled to 100 °C and maintained for 30 min. Then, NH_3 (10%, He) was adsorbed to the sample for 60 min, followed by a flow of He for 20 min. The NH_3 desorption from the samples was detected, while the samples were heated from 100 to 600 °C at 10 °C/min.

The BET surface areas of the samples degassed at 350 °C for 12 h were determined by the N_2 adsorption−desorption method at −196 °C on a Micromeritics ASAP 2460 surface area and pore size analyzer (Micromeritics Instrument Co., Norcross, Georgia, USA).

2.3. Catalytic Activity Evaluation. Methanol to olefins (MTO) reaction was performed in a fixed-bed microreactor (see Figure S1 in the Supporting Information) at atmospheric pressure. The samples were pressed to slice, crushed, and sieved into 0.4−0.8 μm particle size. 0.8 g samples were introduced into the reactor and conditioned at 450 °C for 1 h using N_2 flow. Then, 80% methanol, preheated to 280 °C, was introduced into the reactor with a weight-hourly space velocity (WHSV) of 3.5 h^{-1}. The reaction products were analyzed by an online gas chromatograph (Agilent GC 7890A) (Agilent Technologies, Santa Clara, California, USA) equipped with flame ionization (FID) and thermal conductivity (TCD) detectors.

3. RESULTS AND DISCUSSION

The XRD patterns of all samples are displayed in Figure 1. In the diagram, we can see that every sample shows an obvious

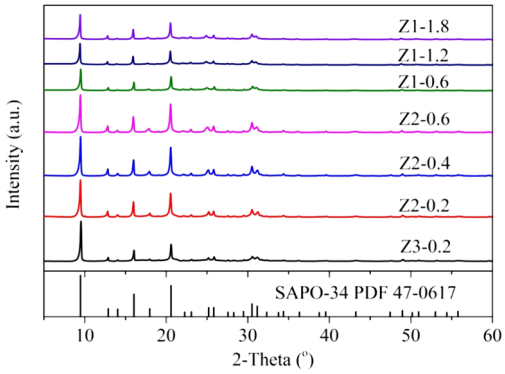

Figure 1. XRD patterns of all of the samples.

diffraction peak of the CHA. Although Z1 samples and Z3-0.2 were prepared by a one-step hydrothermal method, unseparated Z1 samples lead to the coexistence of SAPO-34 and impurities, causing their crystallinity to be much lower than that of Z3-0.2 (see Table 1). No obvious characteristic peaks

Table 1. Composition, Acid, Crystallinity, and Yield of Z2 Samples and Z3-0.2 Sample

		acid (mmol/g)			
samples	molar composition	weak acid	strong acid	crystallinity (%)	yield (%)
Z1-0.6				67.13	
Z1-1.2				62.22	
Z1-1.8				65.75	
Z2-0.2	$Al_{0.501}P_{0.437}Si_{0.062}$	0.491	0.848	78.79	49
Z2-0.4	$Al_{0.488}P_{0.420}Si_{0.092}$	0.814	1.185	83.92	72
Z2-0.6	$Al_{0.471}P_{0.393}Si_{0.136}$	1.033	1.334	83.94	86.5
Z3-0.2	$Al_{0.489}P_{0.446}Si_{0.065}$	0.534	0.912	72.66	41.5

https://doi.org/10.1021/acsomega.4c01266
ACS Omega 2024, 9, 30321−30326

of the impurities have been found in the XRD pattern, because the impurities are amorphous before calcining, and the content is low with full reaction when high silicon has been added.[13] The crystallinity of Z2 samples and Z3-0.2 is also shown in Table 1. Z3-0.2 sample crystallinity is lowest, the crystallinity of Z2 samples increasing with the increasing addition of the Si content.

XRF was used to measure the composition of Z2 samples and Z3-0.2, and the results are shown in Table 1. As we can see from Table 1, with the ratio increase of SiO_2/Al_2O_3 in the crystallized mixture, the silicon content in Z2 samples increased in turn. When the ratio of SiO_2/Al_2O_3 is the same, 0.2, the Si content is almost the same in the Z2-0.2 and Z3-0.2 samples, indicating that the crystallized mixture is completely involved in the reaction and allows for better control of the Si content.

The SEM images of the Z1, Z2, and Z3 samples are shown in Figure 2. As we can see from these images, all samples

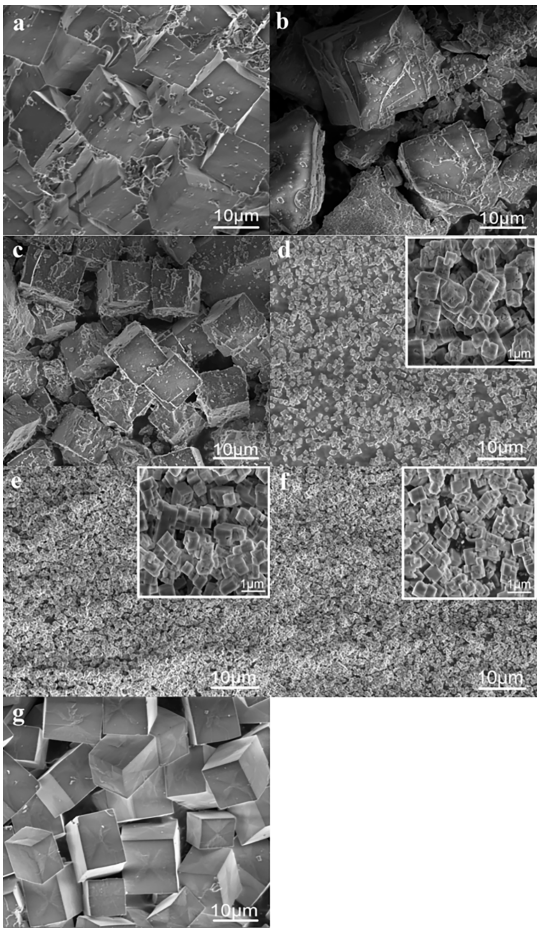

Figure 2. SEM images of Z1-0.6 (a), Z1-1.2 (b), Z1-1.8 (c), Z2-0.2 (d), Z2-0.4 (e), Z2-0.6 (f), and Z3-0.2 (g).

exhibit a cubic-like morphology. Z1 and Z3 samples were prepared by the conventional one-step hydrothermal method, and the size ranged from 10 to 15 μm. Z1 samples were directly dried without separation after hydrothermal treatment; this results in a large number of impurities mixing with the SAPO-34 molecular sieves. Moreover, there was a lot of butterfly-like morphology on the surface of the Z3 sample, but the surface of Z1 samples did not show the same morphology, suggesting that the lower silicon content favors the formation of the butterfly-like morphology. The particle size of Z2 samples ranged from 400 to 900 nm, which is obviously smaller than that of the Z3 sample. Besides, there were a lot of hierarchical hollows on the surface. As the ratio of SiO_2/Al_2O_3 decreased in the crystallized mixture, more hollows appeared on the surface of the Z2 samples but the yield of the samples gradually decreased. In addition, the yield of Z2-0.2 was higher than that of Z3-0.2 (the result is shown in Table 1), which is probably because the addition of the crystallized mixture allows for better dispersion of the raw in the gel and thus facilitates a more adequate reaction.

The acidity of Z2 samples and Z3-0.2 were measured by the NH_3-TPD technique; the result is shown in Figure 3. We can

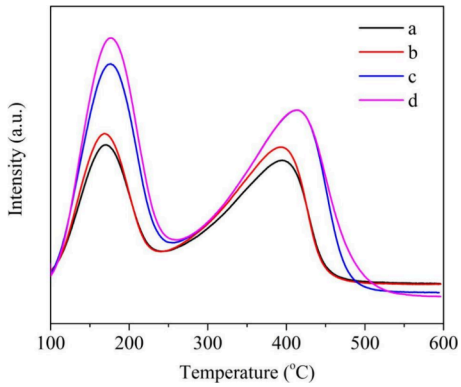

Figure 3. NH_3-TPD profiles of Z2-0.2 (b), Z2-0.4 (c), Z2-0.6 (d), and Z3-0.2 (a).

visually see that all samples show two distinct desorption peaks at 150−250 °C and 350−500 °C, corresponding to the desorption of NH_3 from the weak and strong acid sites. As the ratio of SiO_2/Al_2O_3 increases in the crystallized mixture, the acid amount of the Z2 samples gradually rises. As shown in Table 1, the weak acid amount and the strong acid amount of Z2-0.2 are slightly lower than those of Z3-0.2. At the same time, this also corresponds to the Si content value measured by XRF, which indicates that the Si content affects the acid strength and amount of the molecular sieves.

The N_2 adsorption−desorption test results are shown in Figure 4, and the porosity values are displayed in Table 2. All the samples show the type I N_2 adsorption/desorption isotherm characteristics with almost no hysteresis loop appearing at $P/P0$ = 0.3 to 0.7. However, some upticks above $P/P0$ = 0.8 can be observed in the Z2 samples. It is illustrated that slit mesopores or macropores exist in the Z2 samples. The BJH pore size distributions of the samples are shown in Figure 4b and Figure S2. The Z2 samples have broad pore size distributions ranging from 2 to 100 nm, especially Z2-0.2, so that the distribution is uniform throughout the range. As shown in Table 2, the Z2-0.2 sample with a smaller particle size obtained by two-step hydrothermal synthesis shows higher surface area and volume, especially external surface area and volume, than those of Z3-0.2 with the same SiO_2/Al_2O_3 ratio. Besides, sample Z2-0.6 shows the highest micropore area (1300 $m^2\ g^{-1}$) and microporous volume (0.48 $cm^3\ g^{-1}$) compared to Z2-0.2 (723 $m^2\ g^{-1}$ and 0.28 $cm^3\ g^{-1}$) and Z2-0.4 (825 $m^2\ g^{-1}$ and 0.30 $cm^3\ g^{-1}$). The probable reason is that Si atoms introduced into the framework are beneficial for the formation and stabilization of the pore in the CHA structure.[14] As the Si content increases, the crystallinity

https://doi.org/10.1021/acsomega.4c01266
ACS Omega 2024, 9, 30321−30326

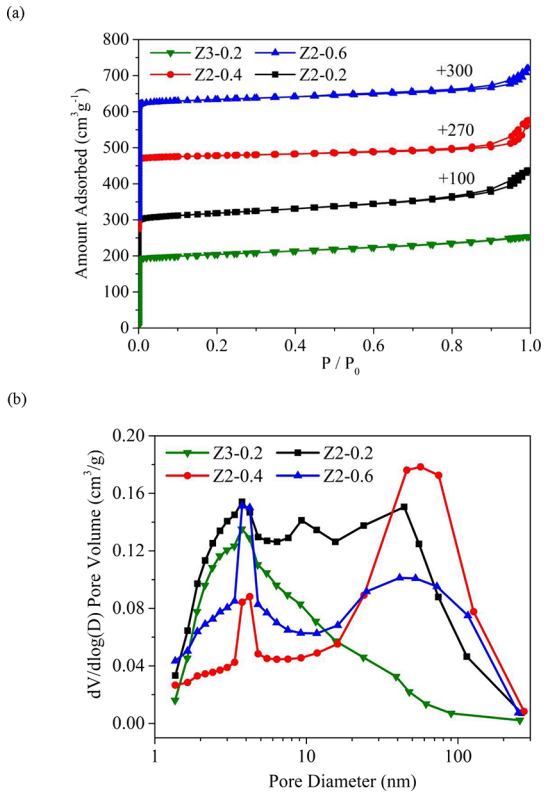

Figure 4. N_2 adsorption−desorption isotherms (a) and the corresponding BJH pore size distributions (b) of Z2 samples and Z3-0.2.

Table 2. Porosity of Z2 Samples and Z3-0.2 Sample

samples	S_{BET} ($m^2 g^{-1}$)	S_{Micro} ($m^2 g^{-1}$)	S_{Ext} ($m^2 g^{-1}$)	V_{total} ($m^3 g^{-1}$)	V_{Micro} ($m^3 g^{-1}$)
Z2-0.2	863	723	140	0.51	0.28
Z2-0.4	881	825	56	0.45	0.30
Z2-0.6	1386	1300	86	0.64	0.48
Z3-0.2	848	742	106	0.39	0.27

and the number of micropores increase. However, further research is needed to explore the relationship between the pore structure and the constituent.

Through the above characterization analysis, the crystallized mixture plays an important role as a Si source and part of raw material for the synthesis of submicrometric and hierarchical hollow SAPO-34. We have made a supposition toward the synthesis of submicrometric and hierarchical hollow SAPO-34, and it is illustrated in Scheme 1. The crystallized mixture was partly dissolved in the precursor solution in the second step. The fully dissolved crystallized mixture was dispersed in the gel as raw, and the incomplete dissolved crystallized mixture was used as a crystal nucleus to induce the formation of SAPO-34. Subsequently, as the crystallization reaction proceeds, the raw material will begin to form crystal nuclei in solution while the nuclei obtained by dissolution begin to grow.[15] At this point, the two form a competitive relationship for the Si source, thereby inhibiting the development of the crystal. Moreover, the gel etches out hierarchical structures due to the slow growth rate of the crystals. Therefore, inhibition of rapid crystal growth facilitates the formation of submicrometer and hierarchical hollow SAPO-34.

The MTO catalytic performances of the Z2 samples and Z3-0.2 sample were tested at 723 K and a methanol WHSV of 3.5 h^{-1} on a fixed-bed reactor. The catalytic lifetimes and selectivities of light olefins are shown in Figure 5. The catalyst lifetime is defined as the reaction duration with more than 99% methanol conversion. As compared with the micron-sized Z3-0.2 sample, the submicrometric and hierarchical hollow Z2-0.2 sample synthesized by the two-step method exhibits a prolonged catalytic lifetime and enhanced selectivity to light olefins. The catalytic lifetime of Z2-0.2 reaches up to 253 min, which is prolonged by about 63 min compared to that of Z3-0.2. The highest light olefin selectivity of Z2-0.2 reaches up to 85.27%, which is nearly 2% higher than that of Z3-0.2. This can be attributed to the smaller particle size and the hierarchical structure, which can help to reduce the length of the intracrystalline diffusion path and overcome diffusion limitations of the reactant and products effectively, thus extending the catalytic lifetime and increasing the selectivity of light olefins. The MTO reaction is a typical acid-catalyzed reaction, and the acidity of the molecular sieve catalyst plays an important role on the lifetime and the selectivity of light olefins in the MTO reaction. As reported by Pajaie et al.,[16] the conversion of methanol to DME occurs mainly on the weak acid sites and there is a great relationship between conversion of DME (and methanol) to light olefins and strong acid sites. Thus, it is more beneficial for the conversion of methanol with stronger acidity of catalysts. However, the stronger acidity and higher acid density in the samples can cause serious side reactions, such as hydrogen transfer reactions and coke deposition. As reported by Dai et al.,[17] the Brønsted acid site density is affected by the Si content. As the Si content increases, the Brønsted acid site density increases and the large

Scheme 1. Possible Process for the Formation of Submicrometric and Hierarchical Hollow SAPO-34.

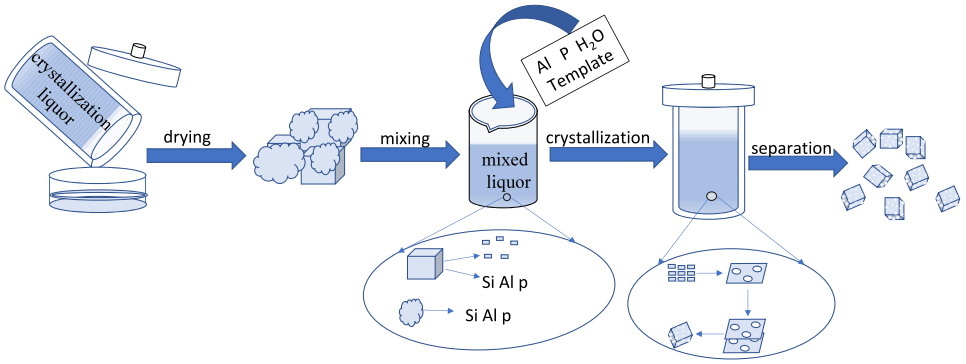

https://doi.org/10.1021/acsomega.4c01266
ACS Omega 2024, 9, 30321−30326

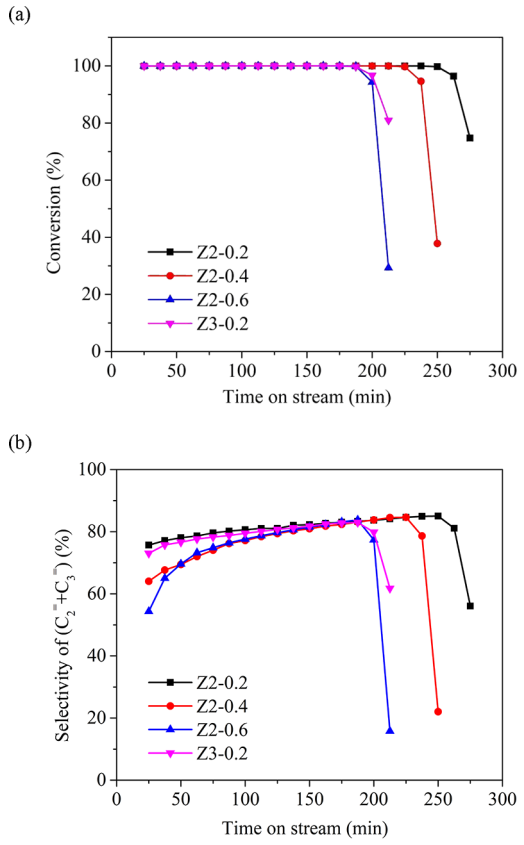

Figure 5. (a) Lifetimes and (b) selectivity of ethylene and propylene.

compounds like poly methylbenzene or even the polycyclic aromatics can be rapidly formed followed by formation of the initial intermediates, which can lead to deactivation of the MTO catalysts eventually. As shown in Table S1, with the increase of Si content in the samples, more methane, ethane, propane, and C_{4+} are generated at the initial stage of the MTO reaction and the lifetime and light olefin selectivity of the samples in the MTO reaction present decreasing trends. Besides, the deposited coke species gradually formed during the reaction can decrease the cage size of the molecular sieves and the acid site density and reduce the generation and diffusion rates of the molecules with larger diameters. Thus, the selectivity of light olefin especially ethylene increases with the reaction time at high methanol conversion. This is more obvious for the samples with stronger acidity and faster coke deposition in the MTO reaction, such as the Z2-0.6 sample. Therefore, the submicrometric and hierarchical hollow SAPO-34 with a low and tunable Si content is an ideal MTO catalyst that can well balance the catalyst activity and deactivation. However, as the ratio of SiO_2/Al_2O_3 in the synthesis gel is as low as 0.18, some big aggregates containing tiny crystals of SAPO-34 and amorphous component can be observed in the SEM images (see Figure S3 in the Supporting Information). Thus, it is difficult to reduce SiO_2/Al_2O_3 further by the two-step hydrothermal synthesis described above. However, it should be noted that the catalytic performance of Z2-0.2 is still superior in the MTO reaction ever reported by our team under similar conditions.[18] Besides, more optimal methods to regulate the efficiency of Si incorporation are being investigated.

4. CONCLUSIONS

Submicrometric and hierarchical hollow SAPO-34 was synthesized by an easy and low-cost two-step hydrothermal method. The crystallized mixture was obtained by direct drying after a first-step hydrothermal reaction. Then, the SAPO-34 product was obtained by adding the crystallized mixture to silicon-free gel and using cheap and common template agents. The acidity of submicrometer and hierarchical hollow SAPO-34 was controlled by the Si content in the crystallized mixture. Moreover, the product synthesized by the two-step hydrothermal method has higher crystallinity, similar composition, and acidity compared to the product synthesized by the common one-step hydrothermal method under the same SiO_2/Al_2O_3 ratio. Compared to the traditional SAPO-34 molecular sieves, the submicrometric and hierarchical hollow SAPO-34 shows a 31% longer catalytic lifetime and 2% higher light olefin selectivity due to the reduced diffusion resistance. Significantly, this study demonstrates a simple synthesis method and provides a new idea for the preparation of small size and hierarchical hollow structures in the synthesis process.

■ ASSOCIATED CONTENT

Supporting Information

The Supporting Information is available free of charge at https://pubs.acs.org/doi/10.1021/acsomega.4c01266.

Fixed-bed microreactor diagram; BJH pore size distributions of Z2 samples and Z3-0.2; SEM images of Z2-0.18; and MTO results over the samples (PDF)

■ AUTHOR INFORMATION

Corresponding Author

Weiping Zhu − *National Institute of Clean-and-Low-Carbon Energy, Beijing 102211, China*; Email: weiping.zhu.a@chnenergy.com.cn

Authors

Zhihui Guo − *National Institute of Clean-and-Low-Carbon Energy, Beijing 102211, China*; orcid.org/0000-0002-4629-0184

Kunlong Liu − *National Institute of Clean-and-Low-Carbon Energy, Beijing 102211, China*

Hui Wei − *National Institute of Clean-and-Low-Carbon Energy, Beijing 102211, China*

Complete contact information is available at: https://pubs.acs.org/10.1021/acsomega.4c01266

Notes

The authors declare no competing financial interest.

■ ACKNOWLEDGMENTS

We thank the China Energy Investment Corporation (GJNY2030XDXM-19-14, S930022016, and S930023085) for supporting this work.

■ REFERENCES

(1) (a) Wilson, S. T., Chapter 4: Phosphate-Based Molecular Sieves: New Structures, Synthetic Approaches, and Applications. In *Stud. Surf. Sci. Catal.*, Čejka, J.; van Bekkum, H.; Corma, A.; Schüth, F., Eds. Elsevier: 2007; Vol. *168*, pp 105−135. (b) Dai, W.; Wang, X.; Wu, G.; Guan, N.; Hunger, M.; Li, L. Methanol-to-olefin Conversion on Silicoaluminophosphate Catalysts: Effect of Brønsted Acid Sites and Framework Structures. *ACS Catal.* **2011**, *1* (4), 292−299. (c) Zhong,

https://doi.org/10.1021/acsomega.4c01266
ACS Omega 2024, 9, 30321−30326

J.; Han, J.; Wei, Y.; Tian, P.; Guo, X.; Song, C.; Liu, Z. Recent Advances of the Nano-hierarchical SAPO-34 in the Methanol-to-olefin (MTO) Reaction and Other Applications. *Catalysis Science & Technology* **2017**, *7* (21), 4905−4923.

(2) (a) Chen, D.; Moljord, K.; Holmen, A. A Methanol to Olefins Review: Diffusion, Coke Formation and Deactivation on SAPO Type Catalysts. *Microporous Mesoporous Mater.* **2012**, *164*, 239−250. (b) Qian, Q.; Vogt, C.; Mokhtar, M.; Asiri, A. M.; Al-Thabaiti, S. A.; Basahel, S. N.; Ruiz-Martínez, J.; Weckhuysen, B. M. Combined Operando UV/Vis/IR Spectroscopy Reveals the Role of Methoxy and Aromatic Species during the Methanol-to-Olefins Reaction over H-SAPO-34. *ChemCatChem.* **2014**, *6* (12), 3396−3408. (c) Sun, Q.; Ma, Y.; Wang, N.; Li, X.; Xi, D.; Xu, J.; Deng, F.; Yoon, K. B.; Oleynikov, P.; Terasaki, O.; Yu, J. High Performance Nanosheet-like Silicoaluminophosphate Molecular Sieves: Synthesis, 3D EDT Structural Analysis and MTO Catalytic Studies. *Journal of Materials Chemistry A* **2014**, *2* (42), 17828−17839.

(3) (a) Yang, G.; Wei, Y.; Xu, S.; Chen, J.; Li, J.; Liu, Z.; Yu, J.; Xu, R. Nanosize-Enhanced Lifetime of SAPO-34 Catalysts in Methanol-to-olefin Reactions. *J. Phys. Chem. C* **2013**, *117* (16), 8214−8222. (b) Yang, M.; Tian, P.; Wang, C.; Yuan, Y.; Yang, Y.; Xu, S.; He, Y.; Liu, Z. A Top-down Approach to Prepare Silicoaluminophosphate Molecular Sieve Nanocrystals with Improved Catalytic Activity. *Chem. Commun.* **2014**, *50* (15), 1845−1847. (c) Zheng, J.; Ding, J.; Jin, D.; Ye, G.; Zhu, K.; Zhou, X.; Yang, W.; Yuan, W. The Tailored Synthesis of nanosized SAPO-34 via Time-controlled Silicon Release Enabled by an Organosilane Precursor. *Chem. Commun.* **2017**, *53* (45), 6132−6135. (d) Sun, Q.; Wang, N.; Guo, G.; Yu, J. Ultrafast Synthesis of Nano-sized Zeolite SAPO-34 with Excellent MTO Catalytic Performance. *Chem. Commun.* **2015**, *51* (91), 16397−16400. (e) Wang, C.; Yang, M.; Li, M.; Xu, S.; Yang, Y.; Tian, P.; Liu, Z. A Reconstruction Strategy to Synthesize Mesoporous SAPO Molecular Sieve Single Crystals with High MTO Catalytic Activity. *Chem. Commun.* **2016**, *52* (38), 6463−6466. (f) Schmidt, F.; Paasch, S.; Brunner, E.; Kaskel, S. Carbon Templated SAPO-34 with Improved Adsorption Kinetics and Catalytic Performance in the MTO-reaction. *Microporous Mesoporous Mater.* **2012**, *164*, 214−221.

(4) van Heyden, H.; Mintova, S.; Bein, T. nanosized SAPO-34 Synthesized from Colloidal Solutions. *Chem. Mater.* **2008**, *20* (9), 2956−2963.

(5) Askari, S.; Halladj, R. Ultrasonic Pretreatment for Hydrothermal Synthesis of SAPO-34 Nanocrystals. *Ultrasonics Sonochemistry* **2012**, *19* (3), 554−559.

(6) Venna, S. R.; Carreon, M. A. Synthesis of SAPO-34 Crystals in the Presence of Crystal Growth Inhibitors. *J. Phys. Chem. B* **2008**, *112* (51), 16261−16265.

(7) Hirota, Y.; Murata, K.; Tanaka, S.; Nishiyama, N.; Egashira, Y.; Ueyama, K. Dry Gel Conversion Synthesis of SAPO-34 Nanocrystals. *Mater. Chem. Phys.* **2010**, *123* (2), 507−509.

(8) (a) Wang, P.; Lv, A.; Hu, J.; Xu, J. a.; Lu, G. The Synthesis of SAPO-34 with Mixed Template and its Catalytic Performance for Methanol to Olefins Reaction. *Microporous Mesoporous Mater.* **2012**, *152*, 178−184. (b) Park, J. H.; Heo, H. S.; Park, Y.-K.; Jeong, K.-E.; Chae, H.-J.; Sohn, J. M.; Jeon, J.-K.; Kim, S.-S. Catalytic Degradation of High-density Polyethylene over SAPO-34 Synthesized with Various Templates. *Korean Journal of Chemical Engineering* **2010**, *27* (6), 1768−1772.

(9) Chen, X.; Vicente, A.; Qin, Z.; Ruaux, V.; Gilson, J.-P.; Valtchev, V. The Preparation of Hierarchical SAPO-34 Crystals via Post-synthesis Fluoride Etching. *Chem. Commun.* **2016**, *52* (17), 3512−3515.

(10) Sun, Q.; Wang, N.; Bai, R.; Chen, X.; Yu, J. Seeding Induced Nano-sized Hierarchical SAPO-34 Zeolites: Cost-effective Synthesis and Superior MTO Performance. *Journal of Materials Chemistry A* **2016**, *4* (39), 14978−14982.

(11) (a) Yang, B.; Zhao, P.; Ma, J.; Li, R. Synthesis of Hierarchical SAPO-34 Nanocrystals with Improved Catalytic Performance for Methanol to Olefins. *Chem. Phys. Lett.* **2016**, *665*, 59−63. (b) Nishiyama, N.; Kawaguchi, M.; Hirota, Y.; Van Vu, D.; Egashira, Y.; Ueyama, K. Size Control of SAPO-34 Crystals and Their Catalyst Lifetime in the Methanol-to-olefin Reaction. *Applied Catalysis A: General* **2009**, *362* (1), 193−199.

(12) (a) Schwieger, W.; Machoke, A. G.; Weissenberger, T.; Inayat, A.; Selvam, T.; Klumpp, M.; Inayat, A. Hierarchy Concepts: Classification and Preparation Strategies for Zeolite Containing Materials with Hierarchical Porosity. *Chem. Soc. Rev.* **2016**, *45* (12), 3353−3376. (b) Li, B.; Hu, Z.; Kong, B.; Wang, J.; Li, W.; Sun, Z.; Qian, X.; Yang, Y.; Shen, W.; Xu, H.; Zhao, D. Hierarchically Tetramodal-porous Zeolite ZSM-5 Monoliths with Template-free-derived Intracrystalline Mesopores. *Chemical Science* **2014**, *5* (4), 1565−1573.

(13) Askari, S.; Bashardoust Siahmard, A.; Halladj, R.; Miar Alipour, S. Different techniques and their effective parameters in nano SAPO-34 synthesis: A review. *Powder Technol.* **2016**, *301*, 268−287.

(14) (a) Han, J.; Yang, G.; Ding, H.; Chen, X. Revealing inherent factors of SAPO-34 zeolites etching towards the fabrication of hierarchical structure. *Microporous Mesoporous Mater.* **2021**, *319*, No. 111067. (b) Yuan, D.; Xing, A.; Miao, P.; Sun, Q.; Cui, L.; Wang, H.; Ma, L.; Chiang, F.; Kong, J. Assembly of Sub-Crystals on the Macroscale and Construction of Composite Building Units on the Microscale for SAPO-34. *Chem. − Asian J.* **2018**, *13* (20), 3063−3072.

(15) Siliveri, S.; Pinnepalli, S. S. K.; Joshi, D.; Chirra, S.; Goskula, S.; Gujjula, S. R.; Oyler, N. A.; Narayanan, V. Investigation on the Promoter-Induced Rapid Non-Aqueous Media Synthesis of SAPO-35 and Methanol-to-olefin Reaction. *ACS Omega* **2021**, *6* (8), 5661−5669.

(16) Sharifi Pajaie, H.; Taghizadeh, M. Optimization of nano-sized SAPO-34 synthesis in methanol-to-olefin reaction by response surface methodology. *Journal of Industrial and Engineering Chemistry* **2015**, *24*, 59−70.

(17) Dai, W.; Cao, G.; Yang, L.; Wu, G.; Dyballa, M.; Hunger, M.; Guan, N.; Li, L. Insights into the Catalytic Cycle and Activity of Methanol-to-olefin Conversion over Low-silica AlPO-34 Zeolites with Controllable Brønsted Acid Density. *Catalysis Science & Technology* **2017**, *7* (3), 607−618.

(18) (a) Guo, L.; Xing, A.; Zhu, W.; Li, F.; Guo, Z., Enhanced methanol-to-olefins(MTO) performance over SAPO-34 molecular sieves synthesized using novel sources of silicon and aluminium. *Clean Energy* **2022**, *6* (3) 528 DOI: 10.1093/ce/zkac031 (b) Guo, L.; Zhu, W.; Xing, A.; Li, F. Synthesis of Low Silica SAPO-34 by In Situ Pretreatment and Its Catalytic Performance in the Methanol-to-Olefins (MTO) Reaction. *Eur. J. Inorg. Chem.* **2023**, *26* (9), e202200787. (c) Guo, L.; Zhu, W.; Xing, A.; Li, F.; Guo, Z. Morphology control of SAPO-34 and its catalytic performance for methanol to olefin reaction. *New J. Chem.* **2022**, *46* (11), 5171−5175.

https://doi.org/10.1021/acsomega.4c01266
ACS Omega 2024, 9, 30321−30326